Current Optics and Photonics
Vol. 3, No. 4, August 2019, pp. 298-303

ISSN: 2508-7266(Print) / ISSN: 2508-7274(Online)
DOI: https://doi.org/10.3807/COPP.2019.3.4.298

Photonic Quasi-crystal Fiber for Orbital Angular Momentum Modes with Ultra-flat Dispersion

Myunghwan Kim and Soeun Kim*

Integrated Optics Laboratory, Advanced Photonics Research Institute, GIST, Gwangju 61005, Korea

(Received April 30, 2019 : revised June 7, 2019 : accepted June 8, 2019)

We propose a photonic quasi-crystal fiber (PQF) for supporting up to 14 orbital angular momentum (OAM) modes with low and ultra-flat dispersion characteristics over the C+L bands. The designed PQF which consists of a large hollow center and quasi structural small air holes in the clad region exhibits low confinement losses and a large effective index separation ($>10^{-4}$) between the vector modes. This proposed fiber could potentially be exploited for mode division multiplexing and other OAM mode applications in fibers.

Keywords : Optical orbital angular momentum, Photonic quasi-crystal fiber, Near zero flattened dispersion
OCIS codes : (060.2270) Fiber characterization; (060.2280) Fiber design and fabrication; (060.5295) Photonic crystal fibers

I. INTRODUCTION

Orbital angular momentum (OAM) modes have been widely investigated due to their unique spiral phase front given as exp($il\varphi$), where l is the topological charge number, and φ is the azimuthal angle [1]. This special phase feature could be utilized in many applications such as optical communications [2-5], quantum information [6, 7], and imaging [8]. In particular, the orthogonality and theoretically unlimited number (i.e. l could be infinity) of the OAM mode justifies it consideration as a new degree of freedom for mode division multiplexing (MDM), which is considered as an alternative to prevail over the increasing data capacity. OAM modes have been successfully demonstrated in free-space using holograms [9], a spiral phase plate [10], and metamaterials [11, 12]. However, the OAM modes based on free-space have limited applications because of the gradual enlargement of these modes with propagation. In this regard, the investigation of OAM modes in optical fibers has attracted significant interest due in part to the long propagation length and ease of mode generation, which could be realized by a combination of the even and odd modes of an identical eigenmode. Recently, terabit-data transmission based on OAM modes in a vortex fiber has been experimentally demonstrated [2, 3]. However, a conventional fiber supports only a few OAM modes.

In order to overcome this problem, OAM modes have been widely investigated in photonic crystal fibers (PCF) such as helically twisted PCFs [13], hexagonal lattice PCFs [14], Kagome lattice PCFs [15], circular PCFs [16-19], and PCFs with As_2S_3 background material [14, 17]. Recently, OAM modes were experimentally demonstrated in a helically twisted PCF [20]. PCFs have been utilized in various fields owing to their unique properties, such as high birefringence [21] and fiber communication [22], and the high index contrast between the air holes and the background material of the PCFs supports many OAM modes. In addition, the PCFs facilitate improved design flexibility compared with conventional fibers in the modification of the mode properties, such as the effective index, dispersion characteristics, and confinement losses. [23].

Although many investigations on OAM modes in PCF have been conducted, the reported results for PCFs indicate large dispersion and dispersion variation with wavelength, which causes signal distortions such as a temporal signal spreading [24]. Therefore, the realization of flat and low

*Corresponding author: sekim@gist.ac.kr, ORCID 0000-0001-5138-4604
Color versions of one or more of the figures in this paper are available online.

dispersion over a wide wavelength range is important for the exploitation of OAM modes for fiber-based high data transmission and multiplexing. In this paper, we propose a photonic quasi-crystal fiber (PQF) to accommodate low and flat dispersion OAM modes over a wide wavelength range. A photonic quasi-crystal is a structure composed of ordered non-periodic triangular and rectangular lattices. PQFs formed by the arrangement of quasi-crystal air holes in the cladding region possess unique properties that are not found in fibers with periodic array air holes [25, 26]. In particular, PQFs can support near zero ultra-flat dispersion over a wide wavelength range [27]. Based on this unique dispersion property of these fibers, we designed a PQF which supports 14 OAM modes with a flat dispersion characteristic over the C+L bands, where the variation of dispersion value for all modes is less than 5 ps/km/nm over C+L bands. Moreover, $HE_{2,1}$ facilitates almost zero dispersion and a very small dispersion variation of 0 to 0.22 ps/km/nm in the range from 1.52 μm to 1.625 μm. It also satisfies a radial single mode condition, a good effective index separation between eigenmodes, and low confinement loss. These properties are essential requirements for OAM multiplexing.

II. STRUCTURE OF THE PROPOSED PQF AND NUMERICAL RESULTS

Figure 1 shows the schematic of the proposed PQF. It consists of a large hollow center (air hole) and quasi-periodic well-ordered 6-air hole layers in the cladding, where a is the period, r_0 is the radius of the center air hole, and r_1 to r_6 are the radii of the air holes in the cladding region. We chose silica as the background material due to its low loss and low nonlinear coefficient. All calculations were performed using a finite element method (FEM) with perfect matched layers (PMLs).

Similar to PCFs, the OAM modes can be supported in PQFs by linear combination of the even and odd symmetric modes of HE or EH, and the $OAM_{l,m}$ mode can be described by the following relations [28].

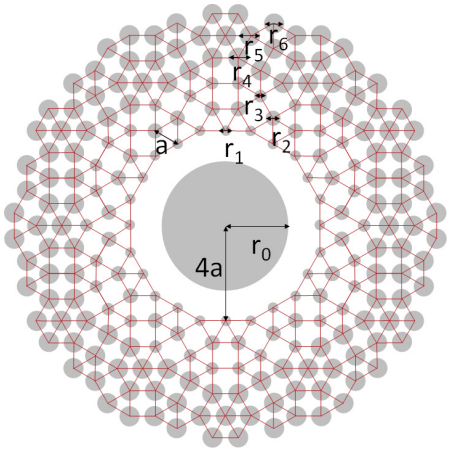

FIG. 1. Schematic of the proposed quasi-crystal fiber. The gray circles represent air holes. a is the distance between neighboring air holes and r_0 to r_6 are the radii of the air holes in the cladding region.

$$OAM_{l,m} = HE^{even}_{l+1,m} \pm jHE^{odd}_{l+1,m} \quad (1)$$

$$OAM_{l,m} = EH^{even}_{l-1,m} \pm jEH^{odd}_{l-1,m} \quad (2)$$

where l is the topological charge number, m is the order of the mode for the radial direction, and the sign of +(-) denotes the right (left) phase rotation.

The PQF was designed to support low and flat dispersion by controlling the size and period of the air holes, and the optimized parameters are a = 1 μm, $r_0 = 2$ μm, $r_1 = 0.353a$, $r_2 = 0.473a$, $r_3 = 0.42a$, and $r_4 = r_5 = r_6 = 0.9a$. Figures 2(a) and 2(b) show the refractive indices of the supported eigenmodes and the effective index difference (Δneff) between the HE and EH modes which have the same order of the OAM mode as a function of wavelength. It should be noted that Δn_{eff} for OAM_1 denotes the effective index difference between the $HE_{2,1}$ mode and the $TE_{0,1}$ mode. As shown in Fig. 2(a), the proposed PQF can support up to $HE_{5,1}$ and $EH_{3,1}$ modes, and thus 14 OAM modes ($|l| \leq 4$) are supported in total; the mode group from the $HE_{2,1}$ to $HE_{5,1}$ modes supports the OAM_l modes from $l = 1$ to $l = 4$,

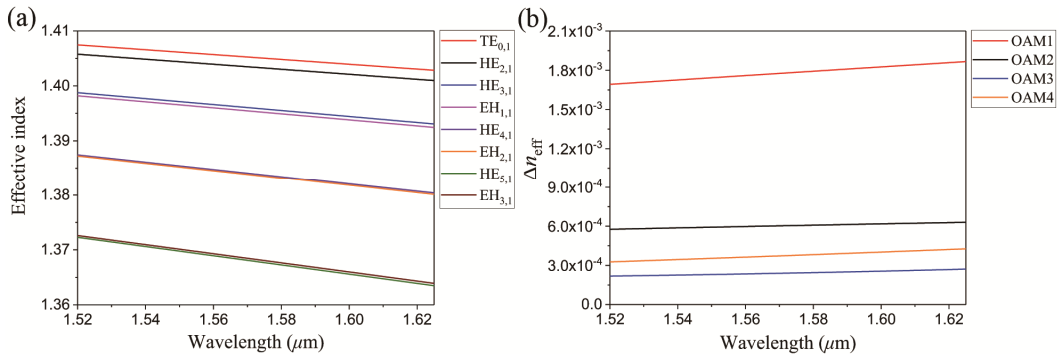

FIG. 2. (a) Effective indices of the eigenmodes and (b) the effective index difference between the same OAM mode orders as a function of wavelength.

respectively, and the mode group from the $EH_{1,1}$ to $EH_{3,1}$ modes supports the OAM_l modes from $l=2$ to $l=4$, respectively. Note that each eigenmode supports right and left wave front rotation direction OAM modes. To exploit the OAM modes in the MDM system, a large effective index separation ($\Delta n_{eff} > 10^{-4}$) between the same ordered OAM modes is necessary. As shown in Fig. 2(b), the Δn_{eff} of all OAM modes increases with an increase of the wavelength, and these are above 10^{-4} over the C+L bands. This means that the OAM modes in the designed PQF maintain a good separation, and thus the OAM modes can be stably transmitted without coupling into the LP modes. It should be noted that the designed fiber satisfies radial single mode ($m < 2$) condition to avoid exciting the higher radial order modes, which could make it difficult to multiplex and de-multiplex the OAM modes.

Figures 3(a) and 3(b) show the electric field intensity and phase distributions , respectively, of the $HE_{3,1}$ (OAM_2) mode. The electric field is well-confined in the silica region with a ring shape, and the phase changes smoothly by 4π in the azimuthal direction. Therefore, the designed PQF adequately supports OAM modes.

We calculated the dispersion characteristics of the eigenmodes as a function of wavelength and the results are shown in Fig. 4(a). The dispersion (D) is calculated using the following equation:

$$D = -\frac{\lambda}{c}\frac{\mathrm{d}^2 \mathrm{Re}(n_{eff})}{d\lambda^2} \tag{3}$$

As shown in Fig. 4(a), all OAM modes have a low and flat dispersion characteristic over the C+L bands. As

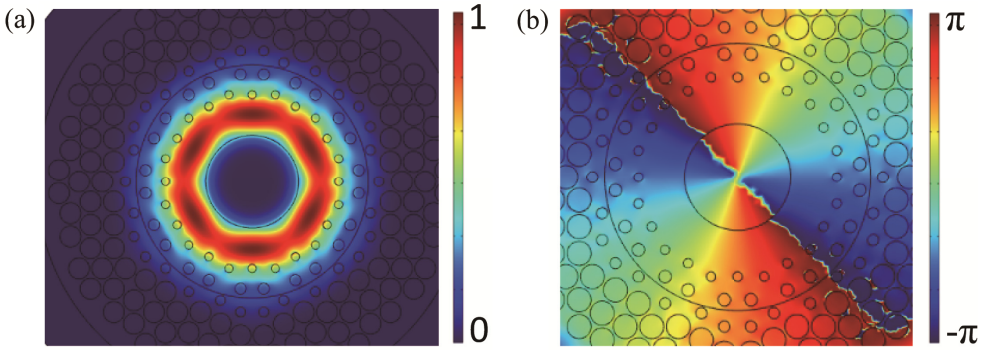

FIG. 3. (a) Electric field intensity and (b) phase distribution of the $HE_{3,1}$ ($OAM_{2,1}$) mode.

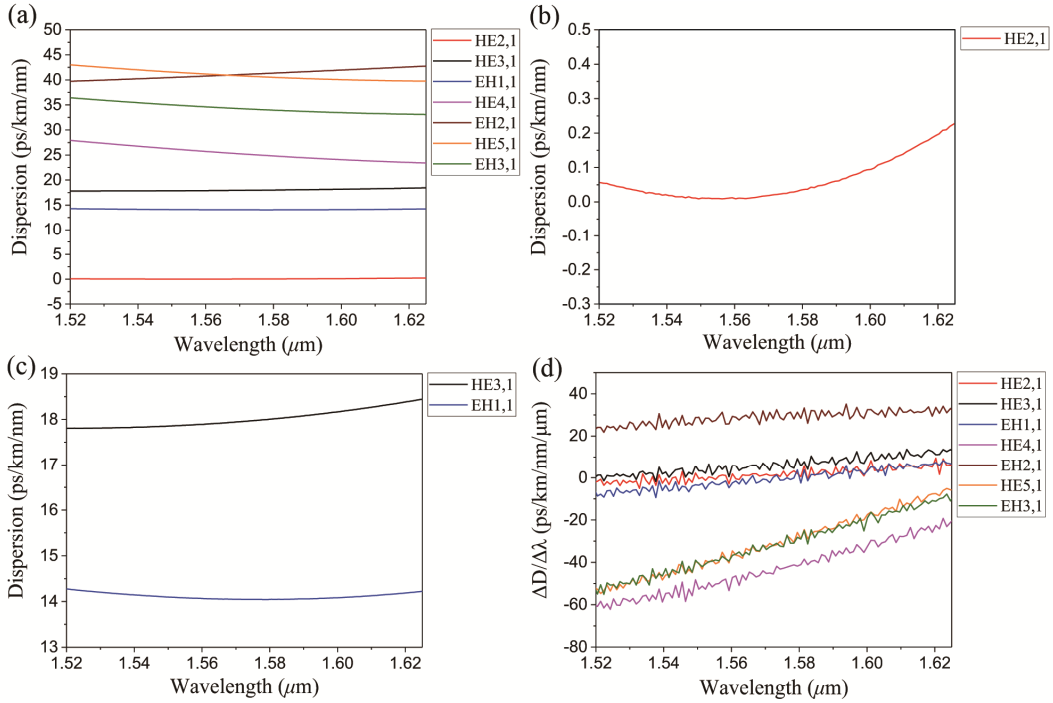

FIG. 4. (a) Dispersion of the eigenmodes as a function of wavelength, and enlarged dispersion of (b) $HE_{2,1}$, (c) $HE_{3,1}$, and $EH_{1,1}$ modes. (d) The differential value of dispersion as a function of wavelength.

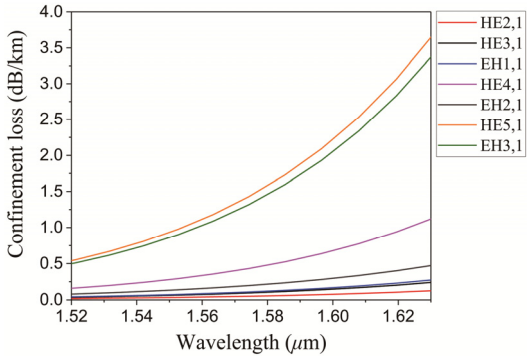

FIG. 5. Confinement loss of the eigenmodes as a function of wavelength.

previously indicated, the photonic quasi crystal structure in the cladding region and the optimized diameters of r_1, r_2, and r_3 account for the flat and low dispersion characteristics, and the resulting variation of the dispersion for all modes is less than 5 ps/km/nm over the C+L bands. The enlarged dispersion value of the $HE_{2,1}$ mode is plotted in Fig. 4(b) to illustrate the specific dispersion variation with respect to wavelength. It can be seen that almost zero and flat dispersion of 0 to 0.22 ps/km/nm in the range from 1.52 μm to 1.625 μm are achieved. Figure 4(c) shows the enlarged dispersion variation of the $HE_{3,1}$ mode and $EH_{1,1}$ mode. The dispersion of these two modes is varied from 14 to 14.3 ps/km/nm and 17.8 to 18.3 ps/km/nm, respectively, in the range from 1.52 μm to 1.625 μm. It should be noted that these dispersion variations are very small compared with reported values for PCFs that support OAM modes [16, 17, 19]. For example, the dispersion values of the OAM modes in circular PCFs are above 100 ps/km/nm for $|l| > 2$ and these values are varied about 20 ps/km/nm over the C+L bands [16]. For a more quantitative investigation of dispersion variation, the wavelength derivative of dispersion is plotted in Fig. 4(d). The derivative value of all the eigenmodes is in the range of -0.06 to 0.04 ps/km/nm^2. In addition, The $HE_{2,1}$ mode shows almost a zero derivative value, and the derivative value of the $HE_{3,1}$ mode and the $EH_{1,1}$ mode are in the range of -0.01 to 0.01 ps/km/nm^2.

We also calculated the confinement loss of the eigenmodes based on the imaginary part of the effective index. Figure 5 shows the confinement loss of eigenmodes as a function of wavelength. It increases with wavelength and the order of the mode due to mode leakage through the cladding. The confinement loss of the $HE_{5,1}$ mode, which has the largest value, is less than ~4 dB/km over the C+L bands. It should be noted that confinement loss can be reduced by increasing the number of air holes in the cladding.

The performance of the OAM modes at 1.55 μm is summarized in Table 1. The designed PQF provides outstanding dispersion characteristics without deterioration of the other mode properties. We also compared the dispersion characteristics of the PQF and the circular PCFs [16, 17], and the result is summarized in Table 2.

The fabrication process of the proposed PQF is more difficult than that of conventional fibers due to the complex structure of PQF. However, we believe that realization of the suggested fiber could be possible using the sol-gel method [29], because this method affords design flexibility

TABLE 1. Summary of the eigenmodes performances at 1.55 μm

		Δn_{eff}	D (ps/km/nm)	dD/dλ (ps/km/nm/μm)	Confinement loss (dB/km)
$HE_{2,1}$	OAM_1	1.74×10^{-3}	1.13×10^{-2}	-0.452	0.034
$HE_{3,1}$	OAM_2	5.93×10^{-4}	17.9	3.36	0.07
$EH_{1,1}$			14.1	-3.565	0.073
$HE_{4,1}$	OAM_3	2.3×10^{-4}	26.2	-52.67	0.286
$EH_{2,1}$			40.5	28.92	0.14
$HE_{5,1}$	OAM_4	3.54×10^{-4}	41.5	-40.37	0.864
$EH_{3,1}$			35	-40.67	0.938

TABLE 2. Comparison of OAM mode performances

OAM Mode		D at 1.55 μm	ΔD at C+L bands (1.52~1.625 μm)
PQF	$HE_{2,1}$	1.13×10^{-2} ps/km/nm	0.22 ps/km/nm
Ref. 16	$HE_{2,1}$	75 ps/km/nm	4.54 ps/km/nm
Ref. 17	$HE_{2,1}$	-280 ps/km/nm	80 ps/km/nm
PQF	$HE_{4,1}$	26.2 ps/km/nm	3.4 ps/km/nm
Ref. 16	$HE_{4,1}$	111.6 ps/km/nm	10 ps/km/nm
Ref. 17	$HE_{4,1}$	-250 ps/km/nm	90 ps/km/nm

in regard to the air hole size and the air hole structure by adjustment of the tuning, drawing speed, and gas pressure.

III. CONCLUSION

We propose a PQF to support OAM modes with low and flat dispersion characteristics. The unique structural property of the PQF and the optimized design of the air holes in the cladding region enable the realization of a very small variation of dispersion (<5 ps/km/nm) and its wavelength derivative (-60 ~ 40 ps/km/nm/μm) over the C+L bands. In particular, the $HE_{2,1}$ mode shows an almost zero and flat dispersion characteristics of D = 0 to 0.22 ps/km/nm, and the $HE_{3,1}$, and $EH_{1,1}$ modes show a small dispersion variation from 14 to 14.3 ps/km/nm and 17.8 to 18.3 ps/km/nm over the C+L bands, respectively. The designed fiber supports up to 14 OAM mode ($|l| \leq 4$), satisfies the radial single mode condition, exhibits low confinement loss, and has good effective index separation between the eigenmodes. The proposed PQF may be applied to various OAM applications, especially in OAM multiplexing.

ACKNOWLEDGMENT

This research was supported by Basic Science Research Program through the National Research Foundation of Korea (NRF) funded by the Ministry of Education (2018 R1D1A1B07049349) and GIST Research Institute (GRI) grant funded by the GIST in 2019.

REFERENCES

1. L. Allen, M. W. Beijersbergen, R. J. C. Spreeuw, and J. P. Woerdman, "Optical angular momentum of light and the transformation of Laguerre-Gaussian laser modes," Phys. Rev. A **45**, 8185 (1992).
2. N. Bozinovic, Y. Yue, Y. Ren, M. Tur, P. Kristenesen, H. Huang, A. E. Willner, and S. Ramachandran, "Terabit-scale orbital angular momentum mode division multiplexing in fibers," Science **340**, 1545-1548 (2013).
3. J. Wang, J. Yang, I. M. Fazal, N. Ahmed, Y. Yan, H. Huang, Y. Ren, Y. Yue, S. Dolinar, M. Tur, and A. E. Willner, "Terabit free-space data transmission employing orbital angular momentum multiplexing," Nat. Photonics **6**, 488-496 (2012).
4. Y. Yan, G. Xie, M. P. J. Lavery, H. Huang, N. Ahmed, C. Bao, Y. Ren, Y. Cao, L. Li, Z. Zhao, A. F. molisch, M. Tur, M. J. Padgett, and A. E. Willner, "High-capacity millimeter-wave communications with orbital angular momentum multiplexing," Nat. Commun. **5**, 4876 (2014).
5. Z. Wang, N. Zhang, and X. C. Yuan, "High-volume optical vortex multiplexing and de-multiplexing for free-space optical communication," Opt. Express **19**, 482-492 (2011).
6. A. Mair, A. Vaziri, G. Weihs, and A. Zeilinger, "Entanglement of the orbital angular momentum states of photons," Nature **412**, 313-316 (2001).
7. Y. Ming, J. Tang, Z. Zhen, F. Xu, L. Zhang, and Y. Lu, "Generation of N00N state with orbital angular momentum in a twisted nonlinear photonic crystal," IEEE J. Sel. Topics Quantum Electron. **21**, 225-230 (2015).
8. S. Furhapter, A. Jesacher, S. Bernet, and M. Ritsch-Marte, "Spiral phase contrast imaging in microscopy," Opt. Express **13**, 689-694 (2005).
9. J. Arlt, K. Dholakia, L. Allen, and M. Padgett, "The production of multiringed Laguerre-Gaussian modes by computer-generated holograms," J. Mod. Opt. **45**, 1231-1237 (1998).
10. K. Sueda, G. Miyaji, N. Miyanaga, and M. Nakatsuka, "Laguerre-Gaussian beam generated with a multilevel spiral phase plate for high intensity laser pulses," Opt. Express **12**, 3548-3553 (2004).
11. Z. Zhao, J. Wang, S. Li, and A. E. Willner, "Metamaterials-based broadband generation of orbital angular momentum carrying vector beams," Opt. Lett. **38**, 932-934 (2013).
12. E. Karimi, S. A. Schulz, I. D. Leon, H. Qassim, J. Upham, and R. W. Boyd, "Generating optical orbital angular momentum at visible wavelengths using a plasmonic metasurface," Light: Sci. Appl. **3**, e167 (2014).
13. G. K. L. Wong, M. S. Kang, H. W. Lee, F. Biancalana, C. Conti, T. Weiss, and P. St. J. Russell, "Excitation of orbital angular momentum resonances in helically twisted photonic crystal fiber," Science **337**, 446-449 (2012).
14. Y. Yue, L. Zhang, Y. Yan, N. Ahmed, J. Yang, H. Huang, Y. Ren, S. Dolinar, M. Tur, and A. E. Willner, "Octave-spanning supercontinuum generation of vortices in an As_2S_3 ring photonic crystal fiber," Opt. Lett. **37**, 1889-1891 (2012).
15. H. Li, G. Ren, B. Zhu, Y. Gao, B. Yin, J. Wang, and S. Jian, "Guiding terahertz orbital angular momentum beams in multimode Kagome hollow-core fibers," Opt. Lett. **42**, 179-182 (2017).
16. H. Zhang, X. Zhang, H. Li, Y. Deng, X. Zhang, L. Xi, X. Tang, and W. Zhang, "A design strategy of the circular photonic crystal fiber supporting good quality orbital angular momentum mode transmission," Opt. Commun. **397**, 59-66 (2017).
17. Z. Hu, Y. Huang, A. Luo, H. Cui, Z. Luo, and W. Xu, "Photonic crystal fiber for supporting 26 orbital angular momentum modes," Opt. Express **24**, 17285-17291 (2016).
18. G. Zhou, G. Zhou, C. Chen, M. Xu, C. Xia, and Z. Hou, "Design and analysis of a microstructure ring fiber for orbital angular momentum transmission," IEEE Photon. J. **8**, 1-12 (2016).
19. H. Zhang, W. Zhang, L. Xi, X. Tang, X. Zhang, and X. Zhang, "A new type circular photonic crystal fiber for orbital angular momentum mode transmission," IEEE Photon. Technol. Lett. **28**, 1426-1429 (2016).
20. C. Fu, S. Liu, Y. Wang, Z. Bai, J. He, C. Liao, Y. Zhang, F. Zhang, B. Yu, S. Gao, Z. Li, and Y. Wang, "High-order orbital angular momentum mode generator based on twisted photonic crystal fiber," Opt. Lett. **43**, 1786-1789 (2018).
21. Z. Hui, Y. Zhang, and A. Soliman, "Mid-infrared dual-rhombic air hole $GE_{20}Sb_{15}Se_{65}$ chalcogenide photonic crystal fiber with high birefringence and high nonlinearity," Ceram.

Int. **44**, 10383-10392 (2018).
22. Z. Hui and J. Zhang, "Demonstration of 100 Gbit/s optical time-division demultiplexing with 1-to-4 wavelength multi-casting using the cascaded four-wave mixing in photonic crystal fiber with a single control light source," Microw. Opt. Technol. Lett. **56**, 2330-2335 (2014).
23. H. Zhang, X. Zhang, H. Li, Y. Deng, L. Xi, X. Tang, and W. Zhang, "The orbital angular momentum modes supporting fibers based on the photonic crystal fiber structure," Crystals **7**, 286 (2017).
24. X. Zhao, G. Zhou, S. Li, Z. Liu, D. Wei, Z. Hou, and L. Hou, "Photonic crystal fiber for dispersion compensation," Appl. Opt. **47**, 5190-5196 (2008).
25. M. E. Zoorob, M. D. B. Chariton, G. J. Parker, J. J. Baumberg, and M. C. Netti, "Complete photonic bandgaps in 12-fold symmetric quasicrystals," Nature **404**, 740-743 (2000).
26. B. Freedman, G. Bartal, M. Segev, R. Lifshitz, and D. N. Christoet, "Wave and defect dynamics in nonlinear photonic quasicrystals," Nature **440**, 1166-1169 (2006).
27. S. Kim, C. Kee, and J. Lee, "Novel optical properties of six-fold symmetric photonic quasicrystal fibers," Opt. Express **15**, 13221-13226 (2007).
28. C. Brunet, P. Vaity, Y. Messaddeq, S. Larochelle, and L. A. Rusch, "Design, fabrication and validation of an OAM fiber supporting 36 states," Opt. Express **22**, 26117-26127 (2014).
29. R. T. Bise and D. J. Trevor, "Sol-gel derived microstructured fiber: fabrication and characterization," in *Proc. OFC/NFOEC Technical Digest. Optical Fiber Communication Conference* (USA, Mar. 2005), Paper OWL6.